Available online at www.sciencedirect.com

SciVerse ScienceDirect

journal homepage: www.elsevier.com/locate/ijrefrig

Turbulent transport of airborne pollutants in a residential room with a novel air conditioning unit

Di Liu [a], Fu-Yun Zhao [a,b,*], Han-Qing Wang [a], Ernst Rank [b]

[a] School of Civil Engineering, Hunan University of Technology, Zhuzhou, 412007 Hunan, China
[b] Faculty of Civil Engineering and Geodesy, Technical University Munich, Munich 80290, Germany

ARTICLE INFO

Article history:
Received 20 December 2011
Received in revised form
11 April 2012
Accepted 13 April 2012
Available online 23 April 2012

Keywords:
Air conditioner
Heat recovery
Airborne pollutants
Asymptotical solutions

ABSTRACT

Modeling on indoor air quality is performed considering the effect of a new window-type air conditioner, which is a promising way toward compromising energy consumption and residential air environment. Sensitivity analysis of the actual operating situations has been implemented, including the total fresh air supply and the full room air recirculation. The effects of supplying air flow rate, pollutant filtration efficiency, and indoor thermal buoyancy on the airborne pollutant transports are also illustrated. The numerical results demonstrate that the reduction of indoor pollutant levels can be accomplished either by increasing the fresh air ratio, or by increasing filtered removal efficiency, or by increasing the supplying airflow rate, or by decreasing the strength of indoor heating source. The indoor contaminant concentration asymptotically approaches to a small value for the situation of full fresh air supply, which agrees well with the analytical solutions of indoor contaminant concentration under the extreme operations.

Transport turbulent de polluants aéroportés dans une pièce résidentielle munie d'un système de conditionnement d'air innovant

Mots clés : conditionneur d'air ; recupération de chaleur ; polluants aéroportés ; solutions asymptomatiques

1. Introduction

With rising living standards and expectations for better thermal comfort, residential air conditioning is becoming widely accepted as being necessary and routine. However, the increased use of residential air conditioning has a significant impact on the total energy use in residences. A significant number of buildings have become more airtight in modern industrial countries for the purpose of energy conservation. More extensive use of insulation, tighter building design to reduce infiltration and increase ratios of recirculated air helps to conserve energy but cause accumulating of pollutant emitted from the human body or building material in interior spaces (Elkilani and Bouhamra, 2001; Lai and Chen, 2006;

* *Corresponding author*. Faculty of Civil Engineering and Geodesy, Technische Universität München, Arcisstr. 21, D-80290 München, Bavaria, Germany. Tel.: +49 89 289 25058.
E-mail addresses: liudi66@163.com (D. Liu), zfycfdnet@163.com, zhao@bv.tum.de (F.-Y. Zhao).
0140-7007/$ – see front matter © 2012 Elsevier Ltd and IIR. All rights reserved.
doi:10.1016/j.ijrefrig.2012.04.011

Nomenclature

A	sectional area (m^2)
Ar	Archimedes number (Gr Re^{-2})
C	dimensionless concentration
c_p	isobaric specific heat (J kg^{-1} K^{-1})
D	diffusive coefficient (m^2 s^{-1})
g	gravity (m^2 s^{-1})
I_{ox}	turbulent intensity (%)
k	turbulent kinetic energy (m^2 s^{-2})
L	length scale/reference length (m)
P	dimensionless pressure
Pr	Prandtl number
Q	air flow rate (m^3 s^{-1})
q_c	cooling load (w)
r	fresh air ratio
r_e	filtered removal efficiency
Re	Reynolds number
Sc	Schmidt number
Sh	Sherwood number
t	temperature (K)
u_i, u_i'	mean and fluctuating velocity components (ms^{-1})
x, y, z	Cartesian coordinates (m)
X, Y, Z	dimensionless Cartesian coordinates

Greek symbols

ε	turbulent energy dissipation rate (m^2 s^{-3})
ν	kinematics viscosity (m^2 s^{-1})
ν_t	turbulent viscosity (m^2 s^{-1})
β	volume expansion coefficient (K^{-1})
ρ	density (kg m^{-3})

Subscripts

c	cooling
exh	exhaust
fre	fresh air
i, j, k	vector directions in x, y and z
in	indoor
mix	mixing
out	outdoor
recir	recirculation
sup	supply

Superscripts

CO_2	carbon dioxide
HCHO	formaldehyde

Longest et al., 2006; Yu et al., 2009). This usually is not focused when urban energy consumption and ambient environment are simultaneously investigated (Huppert and Sparks, 2006), although building energy consumption has occupied over 30 percent of overall urban energy consumptions.

The generation of contaminants is one of the major contributing factors linked to the poor indoor air quality problem (Yang and Chen, 2001; Béghein et al., 2005; Zhang and Chen, 2006). Plus, indoor contaminant levels are always greater than those of outdoor. Therefore, their levels can be reduced by dilution either through increased fresh air or through increased filtration (Gao and Niu, 2007; Li and Niu, 2007; Haghighat et al., 2008). Aglan (2003) has attributed a mathematical model governing the carbon dioxide generation and decay patterns in buildings with high occupancy levels to identify their air exchange rate and the percent of fresh air. Abadie et al. (2001, 2004) have studied the particle pollution with experiments and one-zone model. The particle transport, deposition and filtration phenomena have been controlled and estimated to evaluate ventilation rate, deposition velocity and filter efficiency. The results showed that the indoor air quality could be improved by sufficient fresh air and a high-efficiency filter.

However, increasing fresh air blindly would result in the extravagance of energy consumption. Furthermore, indoor occupants would feel uncomfortable with high air velocity, i.e., air exchange rate is too high. Thus, meeting the contradiction between energy conservation and comfortable indoor environment is an urgent task for researchers. Many sensitivity studies have been conducted for residences. Wargocki et al. (2004) investigated perceived air quality, Sick Building Syndrome (SBS) symptoms and productivity with air exchange rate of 0.6, 2 or 6 h^{-1} respectively, which is typically found in office buildings around the world (Bolashikov and Melikov, 2009). Kuwait researchers concluded that air exchange rates, in Kuwait residences, is the range of 0.15–0.27 h^{-1} for infiltration, 0.25–0.7 h^{-1} through HVAC system and greater than 1.0 h^{-1} and up to 1.7 h^{-1} in case of openings (Bouhamra et al., 1998; Elkilani and Bouhamra, 2001). A 5.16 m × 3.65 m × 2.44 m model room with air exchange rate 4 h^{-1} also has been investigated analytically and numerically (Yang and Chen, 2001).

The fresh air and recirculation air were mixed directly to reduce the indoor pollutant levels with good energy efficiency (Bouhamra et al., 1998; Buhamra et al., 1998; Bouhamar and Elkilani, 1999; Elkilani and Bouhamra, 2001). However, the waste heat of indoor exhaust air has not been deserved in their work. Sensible and latent heat is discharged to the surrounding environment unconsciously. Actually, it can be recovered, hence, by the installation of heat transfer equipment for the recovery of waste heat (Fehrm et al., 2002; Nguyen et al., 2005; Liu et al., 2006, 2007, 2008a, 2010a; Liang et al., 2010). The most practical way of achieving acceptable quality with suitable energy consumption is to allow maximum outside air intake compared to minimum cooling load through waste heat recovery facility to inhibit flush-accumulated levels of indoor contaminants. Refer to the widely used window-type air conditioner in residential buildings for its simplicity and convenience, of which the supply diffuser is often located at window side adjacent to return grill. It is meaningful for us to find a good solution to maintain a comfortable indoor air environment with the premise of minimum energy consumption. A novel window-type air conditioner has been developed with a heat recovery facility to pre-cooling/heating fresh outdoor air with exhaust indoor air. The objective of this new facility is to reduce energy consumption and dilute indoor pollutant simultaneously (Liu et al., 2006, 2010a, 2007).

Present work aims to identify the optimal air conditioning system of achieving a comfortable indoor air environment with the lowest cost of energy. Three-dimensional simulation is performed to evaluate the airflow and contaminant distribution in a building equipped with that novel window-type air conditioner. A large range of parameters, including supplying air speed, fresh air ratio, filtered removal efficiency and thermal buoyancy are numerically investigated. The spatial distribution of contaminant concentration, average volumetric pollutant level, and emission rate are adopted to evaluate the indoor air environment. Following that, the analytical expression of the indoor pollutant concentration is presented as a function of the air conditioner recirculation and fresh air introduced. Finally, the appropriate control strategy for dilution indoor pollutant is examined.

2. Model structure

2.1. *The novel window-type air conditioner with heat recovery facility*

The window-type air conditioner is type of KCR-30, and composed of two parts: an indoor unit and an outdoor unit. Under refrigerating operation, the heat transfer coil at the outdoor unit behaves as an air-cooled condenser. Cooling air is drawn in by a propeller fan, passes through the condenser coil, and carries away the latent heat from refrigerant condensation. Under heating mode operation, the same principle works only the internal tube refrigerant reverses the rotating direction. The novel window-type air conditioner considered here is a fan-assisted stack with pre-cooling of supply air by heat exchange between the indoor exhausting air and outdoor fresh air shown in left frame of Fig. 1(a) (Liu et al., 2006, 2010a). The pre-cooled fresh air effusing from the port 5 in Fig. 1(a) mixes with recirculating air before flowing into the evaporator. The cooling air is supplied to the room. The heat recovery facility is composed of stack heat exchanger and buffer tank. The alumina finned-flat heat exchangers were slapped each other, through which fresh air and exhausting air flow. The objective of the fins is to enlarge heat exchanging area, and then enhance heat transfer. This crossing flow type can make the most of the indoor waste heat to pre-cooling/heating fresh air. The buffer tank is adopted to reorganize the fluid flow. An insulated board was located in the middle of the tank, which can avoid mixing of these two fluids. In order to fit the heat recovery facility on the window-type air conditioner, two ports were adapted with the buffer tank outlets. Insulation is also needed between the heat recovery facility and the window-type air conditioner to reduce heat transfer to surrounding environment.

The experimental results show that the energy saving efficiency could approach to 80%, thus the fresh air ratio could increase greater than that of the traditional HVAC system (Liu et al., 2006). The usual designed fresh air ratio for HVAC systems is about 0.33 (Hays et al., 1995). However, for this novel window-type air conditioner, the fresh air ratio could increase to 0.5 with no extra energy consumption. The supplying, recirculation and exhaust grilles are the same dimensions of 0.4 m × 0.5 m.

As shown in Fig. 1(b), a cubic enclosure (4.0 m × 4.0 m × 4.0 m) slot-ventilated by the novel window-type air conditioner forms the subject of the present study. A discrete contaminant source (1.2 m × 1.2 m) is located on the center of the floor, which is assumed emitting two pollutants simultaneously for constant concentration. Carbon dioxide and formaldehyde have been selected as representative indoor pollutants for this numerical simulation. The heat source of the same location and size with the pollutant source is also presented, and its surface temperature is higher than the supplying cooling air.

2.2. *Energy analysis*

As illustrated in Fig. 1(c), the novel window-type room air conditioner with heat recovery facility is designed to accommodate certain ratio (fresh air ratio r) between fresh air flow rate Q_{fre} and the total air flow rate of fresh air and recirculation ($Q_{sup} = Q_{fre} + Q_{recir}$). The set point for that ratio depends on the design parameters of heat recovery facility to provide the required indoor temperature. It also determines the cooling load or heating load of the new window-type room air conditioner. Actually, as illustrated in Fig. 1(c), outdoor temperature is assumed higher than indoor temperature such that energy balance of the heat recovery facility about fresh air and exhausting air can be performed below

$$Q_{fre} \cdot c_{p\ fre} \cdot (t_{out} - t_{fre.in}) = Q_{exh} \cdot c_{p\ exh} \cdot (t_{exh.out} - t_{in}) \quad (1)$$

Where Q_{exh} represents the exhausted airflow rate by the system. For airflow balance

$$Q_{fre} + Q_{recir} = Q_{exh} + Q_{recir} \quad (2)$$

As a result

$$Q_{fre} = Q_{exh} \quad (3)$$

Assuming constant heat capacity for air in the range of the studied temperatures, Eq. (1) can be further written as

$$t_{out} - t_{fre.in} = t_{exh.out} - t_{in} \quad (4)$$

As expected, the temperature difference would be asymptotically approaching to $t_{out} - t_{in}$ for ideal situation. Additionally, the efficiency of the heat recovery facility ($0 < \varepsilon < 1$) can be defined as

$$\varepsilon = \frac{t_{out} - t_{fre.in}}{t_{out} - t_{in}} \times 100\% = \frac{t_{exh.out} - t_{in}}{t_{out} - t_{in}} \times 100\% \quad (5)$$

Now, energy balance is achieved around the mixing point of the pre-cooling fresh air and recirculation, which could be mathematically expressed as

$$Q_{fre} \cdot c_{p\ fre} \cdot (t_{fre.in} - t_{ref}) + Q_{recir} \cdot c_{p\ recir} \cdot (t_{in} - t_{ref}) = (Q_{fre} + Q_{recir}) \cdot c_p \cdot (t_{mix} - t_{ref}) \quad (6)$$

Using $t_{ref} = 273$ K, the aforementioned equation becomes

$$\frac{Q_{fre}}{Q_{sup}} \cdot t_{fre.in} + \frac{Q_{recir}}{Q_{sup}} \cdot t_{in} = t_{mix} \quad (7)$$

Recalling the definition of fresh air ratio, $r = Q_{fre}/Q_{sup}$, the Eq. (7) is rewritten as

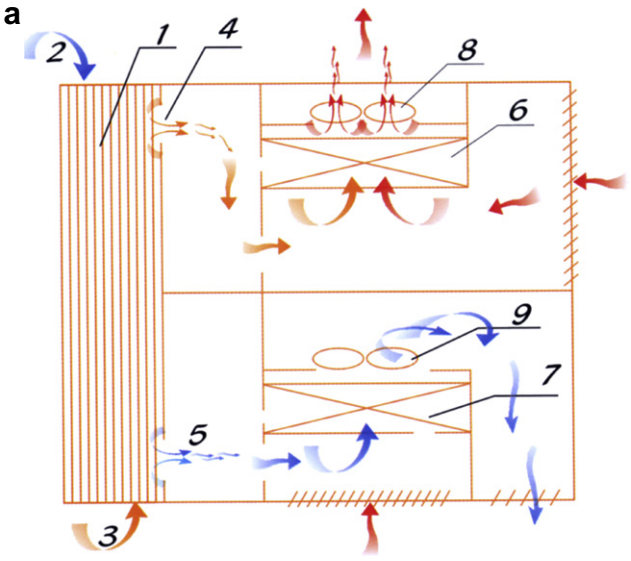

1. Heat recovery facility; 2. Fresh air intake; 3. Indoor exhaust gas inlet; 4. Indoor exhaust gas outlet; 5. Supply air port; 6. Condenser; 7. Evaporator; 8. Supply fan; 9. Exhaust fan

Schematic diagram of the cutting mid-section of the novel window-type air conditioner

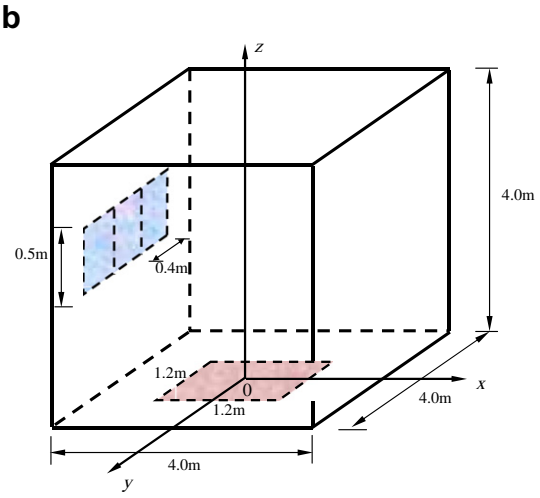

Schematic diagram of the air-conditioning vented room

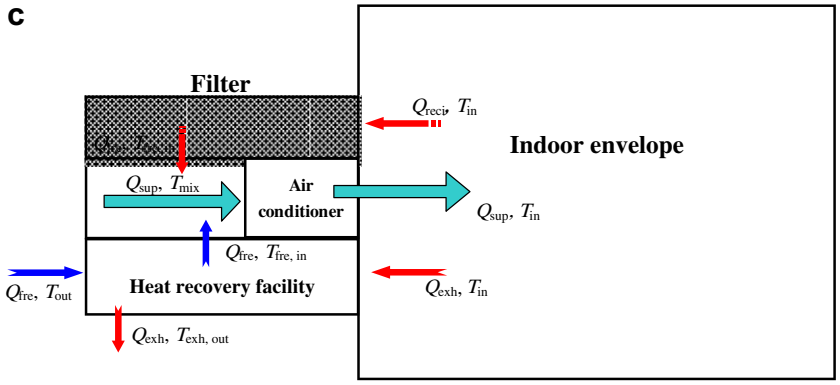

Schematic diagram for indoor envelope with novel window-type air conditioner

Fig. 1 – Schematic diagrams of the indoor envelope with (a) a novel window-type air conditioner; (b) the air conditioning room; and (c) the cutting section of the novel window-type air conditioner.

$$r \cdot t_{fre.in} + (1 - r) \cdot t_{in} = t_{mix} \quad (8)$$

For the whole ventilated room, the cooling load (q_c) is determined by the relation

$$q_c = Q_{sup} \rho \cdot c_p (t_{mix} - t_{in}) \quad (9)$$

Substituting Eqs. (4), (5) and (8) to Eq. (9), the following relation can be obtained

$$q_c = Q_{sup} \cdot \rho \cdot c_p \cdot r \cdot (1 - \varepsilon)(t_{out} - t_{in}) \quad (10)$$

The above equation demonstrates that the cooling load is a function of fresh air ratio r and efficiency of heat recovery facility ε for constant supply airflow rate and temperature difference of outdoor and indoor. The cooling load increases with increasing of fresh air ratio and decreasing of efficiency of heat recovery facility.

2.3. *Mathematical model for fluid flow and pollutant transport*

A computational fluid dynamics code was developed to solve the room airflow. The mathematical model used for continuity, momentum, energy and constituent conservation equations are given as follows (Versteeg and Malalasekera, 1996; Moureh and Flick, 2004, 2005; Smale et al., 2006; Moureh et al., 2009; Liu et al., 2010b).Continuity equation

$$\frac{\partial}{\partial x_i}(\rho \overline{u_i}) = 0 \quad (11)$$

Momentum equation

$$\frac{\partial}{\partial x_j}\left(\overline{u_i u_j}\right) = -\frac{1}{\rho}\frac{\partial p}{\partial x_i} + \frac{\partial}{\partial x_j}\left(\nu \frac{\partial \overline{u_i}}{\partial x_j} - \overline{u_i' u_j'}\right) + \beta(\bar{t} - t_0) g_i \quad (12)$$

Energy conservation

$$\frac{\partial \overline{u_j t}}{\partial x_j} = \frac{\partial}{\partial x_j}\left(D_t \frac{\partial \bar{t}}{\partial x_j} - \overline{u_j' t'}\right) \tag{13}$$

Constituent equation

$$\frac{\partial}{\partial x_j}\left(\overline{u_j c}\right) = \frac{\partial}{\partial x_j}\left(D_c \frac{\partial \bar{c}}{\partial x_j} - \overline{u_j' c'}\right) \tag{14}$$

The Reynolds stresses $\overline{u_i' u_j'}$ and the scalar transport terms appearing in the above Eqs. (12)–(14) should be predicted by the appropriate turbulence modeling. For the case investigated, RSM turbulence modeling closure (Reynolds stress equation model) has been employed for unknown Reynolds stresses and mass fluxes.

A full RSM closure generally consists of six transport equations for the Reynolds stresses – three transport equations for the turbulent fluxes of each scalar property and one transport equation for the dissipation rate of turbulence energy. The Reynolds-stress-transport equations include the diffusion, production, and pressure-strain terms. To obtain the transport equation for Reynolds turbulent stress we multiply the i-component Navier–Stokes equation for the instantaneous velocity $(\overline{u_i} + u_i')$ by the fluctuation u_j'. We then add u_i' times the equations for $(\overline{u_i} + u_i')$ and average

$$\overline{u_k}\frac{\partial \overline{u_i' u_j'}}{\partial x_k} = -\frac{\partial}{\partial x_k}\left[\overline{u_i' u_j' u_k'} + \frac{p}{\rho}\left(\delta_{kj} u_i' + \delta_{ik} u_j'\right) - \nu \frac{\partial\left(\overline{u_i' u_j'}\right)}{\partial x_k}\right] + G_{ij} + \overline{\frac{p}{\rho}\left(\frac{\partial u_i'}{\partial x_j} + \frac{\partial u_j'}{\partial x_i}\right)} - 2\nu \overline{\frac{\partial u_i'}{\partial x_k}\frac{\partial u_j'}{\partial x_k}} \tag{15}$$

Where $G_{ij} = -\overline{u_i' u_k'}\frac{\partial \overline{u_j}}{\partial x_k} - \overline{u_j' u_k'}\frac{\partial \overline{u_i}}{\partial x_k}$ represents the production term. The diffusive transport term is represented by a simplified form of the generalized gradient diffusion hypothesis as

$$-\frac{\partial}{\partial x_k}\left[\overline{u_i' u_j' u_k'} + \frac{p}{\rho}\left(\delta_{kj} u_i' + \delta_{ik} u_j'\right) - \nu \frac{\partial\left(\overline{u_i' u_j'}\right)}{\partial x_k}\right] = \frac{\partial}{\partial x_k}\left(\frac{\nu_t}{\sigma_k}\frac{\partial}{\partial x_k}\left(\overline{u_i' u_j'}\right)\right) \tag{16}$$

The pressure-strain term consists of the linear return-to-isotropy and is modeled as

$$\overline{\frac{p}{\rho}\left(\frac{\partial u_i'}{\partial x_j} + \frac{\partial u_j'}{\partial x_i}\right)} = -C_1 \frac{\varepsilon}{k}\left(\overline{u_i' u_j'} - \frac{2}{3}\delta_{ij} k\right) - C_2\left(G_{ij} - \frac{2}{3}\delta_{ij} G\right) \tag{17}$$

Where the term G is defined as $0.5G_{ii}$.The dissipation term is assumed isotropic, and is approximated by the following relation

$$2\nu \overline{\frac{\partial u_i'}{\partial x_k}\frac{\partial u_j'}{\partial x_k}} = \frac{2}{3}\delta_{ij}\varepsilon \tag{18}$$

Where the dissipation rate ε is computed via the following transport equation

$$\overline{u_j}\frac{\partial \varepsilon}{\partial x_j} = C_{\varepsilon 1}\frac{\varepsilon}{k}\left(-\overline{u_i' u_j'}\frac{\partial \overline{u_i}}{\partial x_j}\right) - C_{\varepsilon 2}\frac{\varepsilon^2}{k} + \frac{\partial}{\partial x_j}\left(\left(\nu + \frac{\nu_t}{\sigma_\varepsilon}\right)\frac{\partial \varepsilon}{\partial x_j}\right) \tag{19}$$

The eddy viscosity concept is adopted to relate the eddy viscosity ν_t to the turbulent kinetic energy k and its rate of dissipation ε, i.e., $\nu_t = C_\mu k^2/\varepsilon$. The empirical coefficients appearing in the aforementioned equations or relations such as C_1, C_2, $C_{\varepsilon 1}$, $C_{\varepsilon 2}$, C_μ, σ_k and σ_ε are maintained at 1.80, 0.60, 1.44, 1.92, 0.09, 1.00 and 1.30 respectively.The turbulent heat flux is given as

$$\overline{u_j' t'} = -\frac{\nu_t}{\mathrm{Pr}_t}\frac{\partial \bar{t}}{\partial x_j} \tag{20}$$

The turbulent mass flux is expressed as

$$\overline{u_j' c'} = -\frac{\nu_t}{\mathrm{Sc}_t}\frac{\partial \bar{c}}{\partial x_j} \tag{21}$$

Numerical difficulties and errors would arise because the large parametric values associated with three-dimensional convective flow cause the terms to have disparate magnitudes that require more computer storage and also lead to calculations of large differences of small numbers, or vice versa. Recognizing that the convection term must maintain balance and considering the ranges of governing parameters in the present work, the following dimensionless variables are used

$$(X, Y, Z) = (x, y, z)/L_0\ ,\ (U, V, W)/U_0\ ,\ P = p/\rho U_0^2,\ K = \frac{k}{U_0^2},\ E = \frac{\varepsilon L_0}{U_0^3} \tag{22a}$$

$$C_{CO_2} = \left(c^{CO_2} - c_0^{CO_2}\right)/\Delta c_0^{CO_2},\ C_{HCHO} = \left(c^{HCHO} - c_0^{HCHO}\right)/\Delta c_0^{HCHO},\ T = (t - t_0)/\Delta t_0 \tag{22b}$$

Where L_0, U_0, Δc_0 and Δt_0 are the scales for length, velocity, constituent and temperature respectively. In the present study, the half height of the room ($L_0 = 2.0$ m) and the uniform supplying velocity ($U_0 = U_{sup}$), concentration difference between the pollutant source and fresh air, temperature difference between the heat source and cooling supply air are taken as L_0, U_0, Δc_0 and Δt_0 respectively. Numerical results of the present work are non-dimensional. The control parameters for the aforementioned airflow and pollutant transports are defined as follows

$$\mathrm{Re} = U_0 L_0/\upsilon,\ \mathrm{Ar} = (g\beta\Delta t_0 L_0)/U_0^2,\ \mathrm{Pr} = \upsilon/D_t,\ \mathrm{Sc}_1(CO_2) = \upsilon/D_{c1},\ \mathrm{Sc}_2(\mathrm{HCHO}) = \upsilon/D_{c2} \tag{23}$$

Reynolds number (Re) expresses the relative importance of inertial forces and viscous forces, whereas Archimedes number (Ar) represents the relative strengths of thermal buoyancy forces and inertial forces. Prandtl number of air at room temperature is maintained at 0.71. For air mixtures, Béghein et al. (1992) pointed out that the chemical species of most common interest have Schmidt numbers in the range of 0.1–10. In this study, values of Schmidt number with 0.2 (Sc_1 for CO_2) and 2.0 (Sc_2 for formaldehyde) have been considered.

2.4. General boundary conditions

The non-slip and impermeable conditions are imposed on all the solid walls. The flow through the inlet port is purely horizontal (forming a jet), and the velocity components, kinetic energy of turbulence, the energy dissipation rate and concentration of this stream are uniform over the cross-section of the inlet port

$$V_{sup} = W_{sup} = 0,\ U_{sup} = 1.0 \tag{24}$$

Where U_{sup} represents the mean stream wise longitudinal velocity. The inlet kinetic energy of turbulence and the energy dissipation rate can be obtained as

$$K_{sup} = 3/2(U_{sup}I_{ox})^2,\quad E_{sup} = \left(C_{\mu}^{0.75}K_{sup}^{1.5}/0.07D_H\right) \tag{25}$$

Where $I_{ox} = 10\%$ represents the turbulence intensity of the X-component of velocity at the inlet as obtained from experiments. D_H represents dimensionless hydraulic diameter of the inlet section. The turbulence is assumed to be isotropic, $\overline{u_i'u_j'} = 2/3k_0\delta_{ij}$.

The outlet boundary condition (zero flux) was chosen for numerical convenience. The aforementioned turbulence model is only valid in fully turbulent regions. Close to the wall, where viscous effects become dominant, these models are used in conjunction with wall functions. For this study, the conventional equilibrium logarithmic law governing the wall is used (Liu et al., 2010b).

2.5. Boundary conditions for the novel window-type air conditioner

The airflow rate and pollutant concentration of the mixed air in the window unit are quantified by mass and constituent conservations, respectively, due to the well-mixed assumption. The airflow rate balance for the novel air conditioner with heat recovery facility is expressed as

$$Q_{sup} = Q_{recir} + Q_{exh} \tag{26}$$

Considering the average jet flow, Eq. (26) could be further written as

$$(UA)_{sup} = (UA)_{recir} + (UA)_{exh} \tag{27}$$

Where U represents the average velocity of ports. The area of each grille A is the same, hence, the average velocities of each port can have the following relations

$$U_{sup} = U_{recir} + U_{exh} \tag{28}$$

Recalling fresh air ratio definition

$$r = Q_{fre}/Q_{sup} (0 < r < 1) \tag{29}$$

Therefore, velocities at recirculating and exhausting ports can be defined as

$$U_{recir} = (1-r)U_{sup}, U_{exh} = rU_{sup} \tag{30}$$

Concerning the pollutant boundary conditions, filtration effect should also be taken into consideration. On the basis of the constituent conservation

$$C_{sup}\cdot Q_{sup} = C_{recir}\cdot Q_{recir}(1-r_e) + C_{fre}Q_{fre} \tag{31}$$

Where r_e represents the filtered removal efficiency, whereas C_{recir} and C_{fre} represent the area-averaged contaminant concentrations at recirculating port and outdoor. In terms of non-filtration of carbon dioxide, $r_e = 0$, Eq. (31) is rewritten as

$$C_{sup}^{CO_2} = (1-r)C_{recir}^{CO_2} = (1-r)\frac{\int c_{recir}^{CO_2}dA}{A_{recir}} \tag{32}$$

Considering filtration, the formaldehyde concentration at the supplying port (basing the Eq. (31)) can be obtained as

$$C_{sup}^{HCHO} = (1-r)(1-r_e)C_{recir}^{HCHO} = (1-r)(1-r_e)\frac{\int c_{recir}^{HCHO}dA}{A_{recir}} \tag{33}$$

For these two pollutants, Neumann boundary conditions are imposed at recirculating and exhausting ports

$$\left.\frac{\partial C}{\partial n}\right|_{recir}^{CO_2} = \left.\frac{\partial C}{\partial n}\right|_{exh}^{CO_2} = 0,\ \left.\frac{\partial C}{\partial n}\right|_{recir}^{HCHO} = \left.\frac{\partial C}{\partial n}\right|_{exh}^{HCHO} = 0 \tag{34}$$

Concerning the thermal boundary conditions, all walls are assumed insulated to minimize the heat gain/loss. At the inlet, uniform supply air temperature distribution is assumed at zero, which represents cooling air injection. Neumann boundary conditions also are imposed at recirculating and exhausting ports

$$\left.\frac{\partial T}{\partial n}\right|_{recir} = \left.\frac{\partial T}{\partial n}\right|_{exh} = 0 \tag{35}$$

A simple assumption of constant concentration pollutant source ($C_{source}^{CO_2} = C_{source}^{HCHO} = 1$) is adopted to consider the interfacial mass transfer due to the interaction of the material surface with the adjacent air. Similarly, constant temperature thermal source ($T_{source} = 1$) is imposed.

2.6. Numerical methodology for air flow simulation

The above governing equations are discretized by finite volume method (FVM) on a staggered grid system with three-dimensional system (Patankar, 1980; Versteeg and Malalasekera, 1996). Second-order central difference scheme (CDS) is implemented for the convection and diffusion terms, and deferred-correction is adopted in discretization of convection terms to avoid oscillation (Zhao et al., 2007). The resulting algebraic equations are solved by a line-by-line procedure, combining the tri-diagonal matrix algorithm (TDMA) and the successive over-relaxation (SOR) iteration. The SIMPLE algorithm is used to deal with the linkage between the pressure and the velocity (Patankar, 1980).

Finer meshes were used near the entry, exit, and wall regions. All results presented here were obtained using a 74,088 mesh system. The convergence criteria for each control volume were that the maximum residuals of the mass, momentum, energy and species should all be less than 10^{-5}.

2.7. Model validation

The current numerical method has been successfully used in a series of recent papers, including conjugate heat transfer (Zhao et al., 2007, 2010; Liu et al., 2008b), transient resonant fluid flow (Liu et al., 2008b), natural convection, forced convection and mixed convection in air-mixture enclosure (Liu et al., 2008c, 2010a, 2010b; Zhao et al., 2009), double diffusive natural convection in gaseous enclosures and porous enclosures (Zhao et al., 2008, 2011; Liu et al., 2008d). Experimental validation by authors' PIV rig system could be found in Liu et al. (2010b).

Further, before applying the numerical scenario simulations to the proposed problem, the present turbulent airflow numerical model was verified by a three-dimensional trailer given by Moureh and Flick (2004, 2005), which provides reliable experimental data of velocity. In addition, the blowing and outlet sections are located on the same side at the front of the trailer; which is very similar to the building configuration in our proposed problem. Their experiment was conducted using a reduced scale (1:3.3) model of a trailer with respect to the dimensional Reynolds number ($Re = \rho W_0 D_H/\mu$). The dimensions of this device expressed using the actual scale is represented in Fig. 2(a). The opening height was 0.12 m. The inlet velocity W_0 is 11 m s^{-1}, D_H equals 0.18 m and the kinematic viscosity is 1.5 × 10^{-5} m^2 s^{-1} resulting in a Reynolds

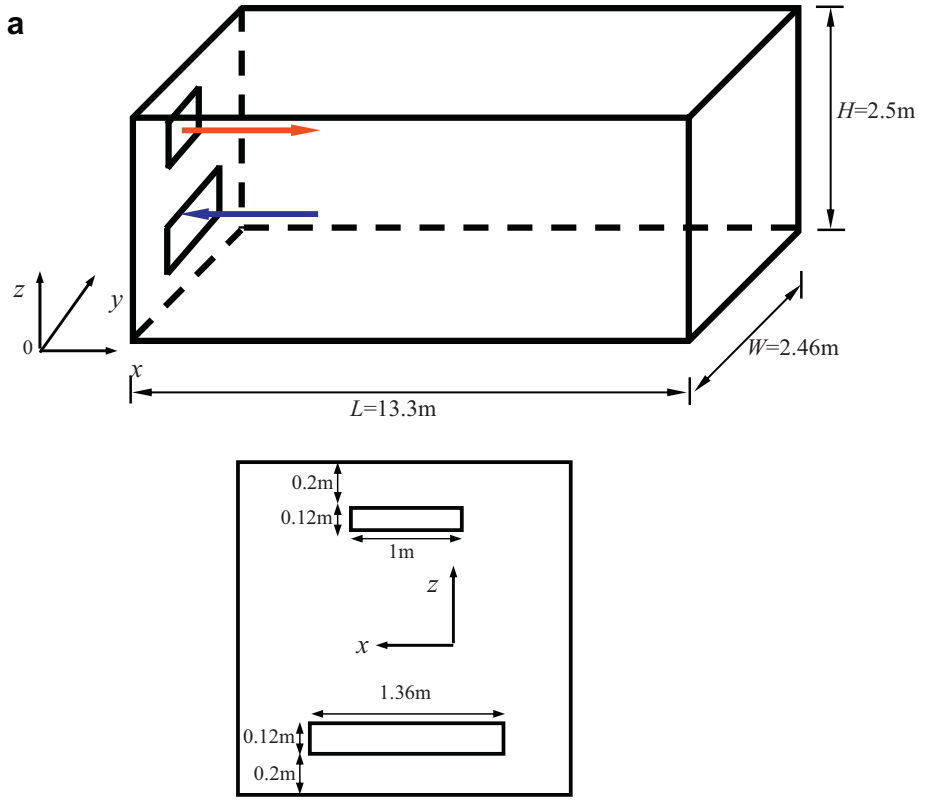

Schematic view of the slot-ventilated enclosure showing inlet and outlet positions

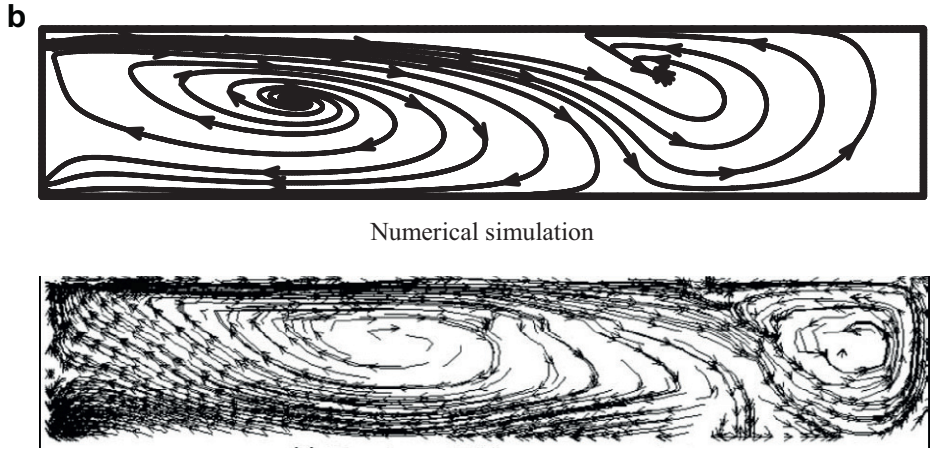

Numerical simulation

Experimental measurement

Airflow pattern on the symmetry plane: comparison between experiment and numerical simulation

Fig. 2 – Airflow measurement in a slot-ventilated enclosure and comparison with benchmark results provided by Moureh and Flick (2005). (a) Schematic view of the slot-ventilated enclosure showing inlet and outlet positions; (b) Airflow pattern on the symmetry plane: comparison between experiment and numerical simulation.

number of 1.3×10^5 in the experiment. The walls of the scale model are made of wood. Only one lateral wall is made of glass to allow internal air velocity measurement using one-dimensional laser Doppler velocimetry (LDV) produced by TSI manufacturer. This system does not interfere with the flow and is able to correctly resolve the sign as well as the magnitude of velocity and to determine mean velocity and its fluctuation. It comprised a 50 mW Laser diode emitting a visible red beam at 690 nm wavelength, a beamsplitter, a Brag cell, a focusing and receiving lens, a pinhole arrangement to collect scattered light and a photomultiplier. Light scattered from particles was captured through the same front lens that the two beams exit from. The air supplied to the model was passed through atomizers and allowed near continuous Doppler signals which were converted into velocity and time. The probe was positioned by a computer controlled traversing arm which provided a resolution of ±0.5 mm in three directions. In their experiments, the decay of the velocity along the enclosure, horizontal and vertical velocity profiles at different longitudinal positions were obtained. In addition to these profiles, 1080 measurements for horizontal and vertical velocities were performed in the whole medium/symmetry plane in order to represent the streamlines and airflow pattern. The measurement scheme used a uniform grid with 0.5 m horizontal intervals and 0.1 m vertical intervals.

Fig. 2(b) depicts the comparisons of streamlines related to the mean flow field on the symmetry plane in the enclosure between experiments and numerical simulation. These flow patterns are consistent with the experimental data of Moureh and Flick (2005). Fig. 3 presents the decay of velocity at the axis. It can be observed that the wall jet separates from the ceiling at approximately $X/L = 8.5/13.3$. The primary recirculation located in the front part of the enclosure delimits the reach and the action of the inlet jet. The results show good agreement of distributions of the simulated and measured data.

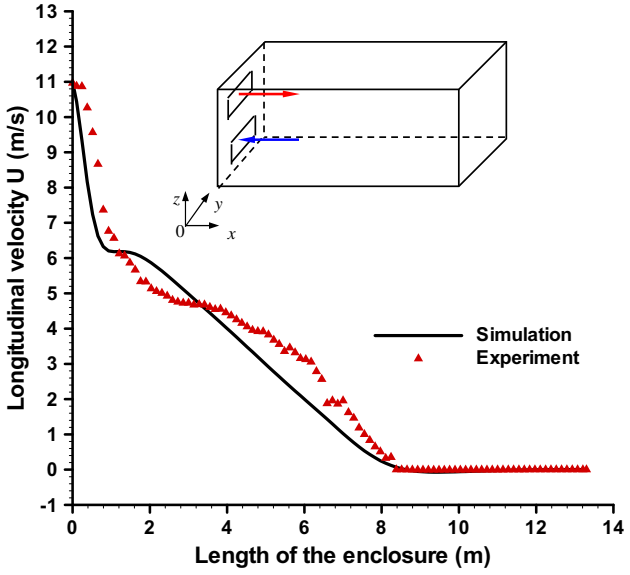

Fig. 3 – Decay of the jet velocity along the enclosure: comparison between experiment and numerical results.

The validation was also carried out through the comparison with the experimental data provided by Koseff and Street (1984). The central component of their facility was a cavity upon which the system supplying the driving force rests. The ratio of the cavity depth D to cavity width B is 1:1 and that of the span L to width B is 3:1. The facility was fabricated from 12.5 mm Plexiglas. The cavity was bounded at the top and bottom by temperature-controlled plates. Shear was imparted to the cavity fluid by the lid, a 0.08 m thick thermally conductive copper belt, supported on and driven by two rollers. Repeated measurements over the period of the experiments showed belt speed to be constant with a drift of 0.5 percent during any particular experiment. Instantaneous velocity measurements, in two orthogonal directions in a vertical plane, were made using a two-component DISA 55X

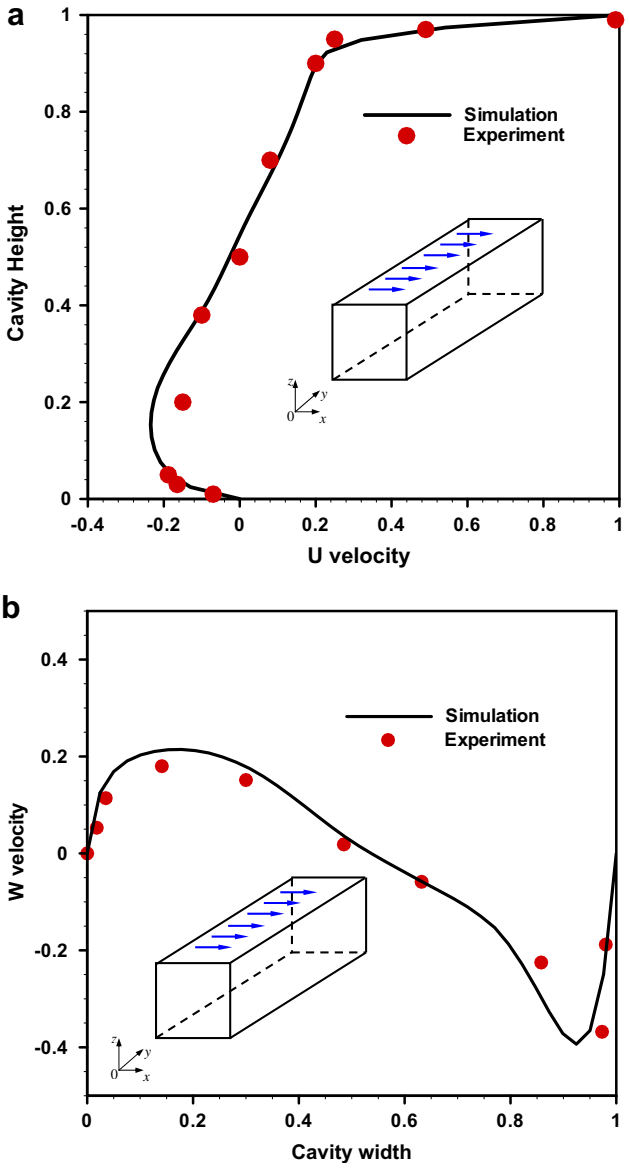

Fig. 4 – Comparison between RSM and experimental results in terms of centerline mean velocity profiles: simulation profile at $Z = 0.28$ plane and experimental data measured at mid-span plane. (a) U velocity, (b) W velocity.

modular optical laser-Doppler-anemometer (LDA) system. The system was equipped with Bragg cell frequency shift and was capable of operating in both forward-scatter and backward-scatter modes. The data was sampled at a rate of 100 Hz by an HP2100A data acquisition system. The absolute accuracy of the system was 0.1 percent of full scale. The uncertainty in the instantaneous velocity measurement ranges from 10 percent at 1 mm s^{-1} to 1 percent at 30 mm s^{-1}.

Comparison between the computed centerline velocity profiles and the experimental results was conducted and shown in Fig. 4. The results indicated that the flow characteristics do not change, as Reynolds number does not exceed 10^4. The averaged error (as compared to the data) was less than 10 per cent.

2.8. *Evaluating parameters*

The average pollutant level is monitored by the volume-averaged pollutant concentration

$$\overline{C} = \frac{1}{V}\int_V C(X,Y,Z)\mathrm{d}X\mathrm{d}Y\mathrm{d}Z \tag{36}$$

In which V is the enclosure volume.

The emission rate can be interpreted as average mass fluxes at the pollutant source, which is given in the non-dimensional term – Sherwood number

$$Sh = \int_{-0.3}^{0.3}\int_{-0.3}^{0.3} -\left[\frac{\partial C}{\partial Z}\right]_{Z=0}\mathrm{d}X\mathrm{d}Y \tag{37}$$

Upon solving the concentration fields, the emission rate (Sherwood number) and the average pollutant level can be obtained directly via the above relations.

3. Sensitivity analysis

Firstly, attention is focused herein on variation of the following parameters without thermal plume effect: supply air speed u_{sup}, fresh air ratio r and filtered removal efficiency r_e. Subsequently, the effect of thermal buoyancy on the contaminant dispersion is discussed.

3.1. *Effect of supply air speed*

The fresh air ratio and the filtered removal efficiency are maintained at 0.5 and 0.8 respectively. For the inlet section, the inlet velocity is in a range of 7.5×10^{-4} m s^{-1}–1.125 m s^{-1} and the kinetic viscosity is 1.5×10^{-5} m^2 s^{-1}, and then all these would result in that the Reynolds number varies from 10^2 to 1.5×10^5. As a result, the resulting air exchange rate is no more than 6.3 h^{-1} such that it can match the practical building ventilation.

The mean supply and recirculation airflow vectors in the building for various supply air speeds are illustrated in Fig. 5(a) and (b), respectively. Observing from Fig. 5(a), there are two main flow patterns in the building, the lower one starting at inlet with high velocity and low concentration level is a clockwise recirculation zone near the floor. The upper counterclockwise vortex forms near the roof. The two zones are directly separated by the supplying jet. The higher momentum results in the longer persisting distance, together with pollutants. After passing over the whole room, pollutants emitted from the floor source are entrained into the clockwise cell and taken away from the building. Simultaneously, pollutants can also be entrained into the recirculating non-clockwise cell and recycling in the building.

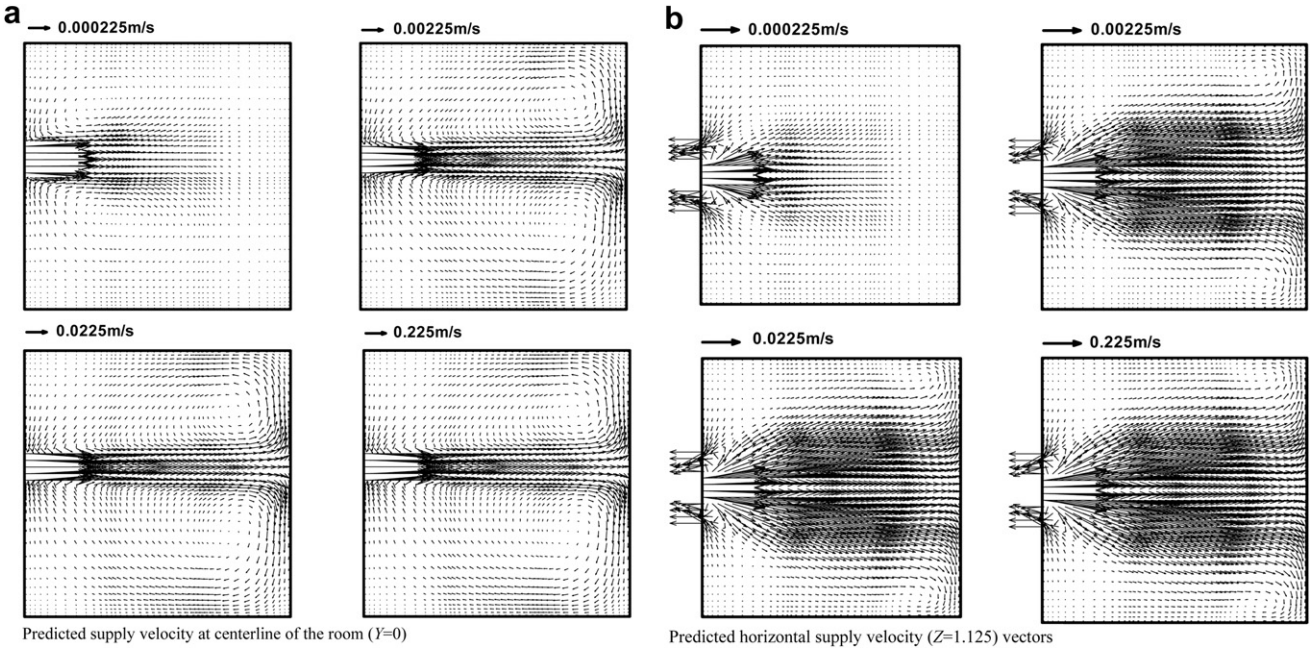

Fig. 5 – Vectors of flow in the building with various supply air speed (represented as reference vector) for fresh air ratio r = 0.5 and filtered removal efficiency r_e = 0.8. (a) Predicted supply velocity at centerline of the room (Y = 0); (b) Predicted horizontal supply velocity (Z = 1.125) vectors.

Figs. 6 and 7 present the normalized steady-state concentration profiles of carbon dioxide and formaldehyde respectively. Fig. 6 presents the carbon dioxide concentration with various supply air speeds, and little dilution occurs in the building with the relatively low supply air speed. For example, the concentration of carbon dioxide is reduced only by ~28% at the middle location ($X = 0$, $Y = 0$, $Z = 1.125$) with $u_{sup} = 7.5 \times 10^{-4}$ m s^{-1}, but by ~59% with $u_{sup} = 0.0075$ m s^{-1}. Dilution is further enhanced to 63% and 76%, respectively, with $u_{sup} = 0.075$ m s^{-1} and 0.75 m s^{-1} at the middle location. For carbon dioxide, with recirculation and non-filtered effects, high concentration level is revealed at the entrance region of the incoming flow for relatively low supply air speed. The concentration at the supply location ($X = -1.0$, $Y = 0$, $Z = 1.125$) are about 0.62 and 0.31 for $u_{sup} = 7.5 \times 10^{-4}$ m s^{-1} and 7.5×10^{-3} m s^{-1}, respectively. But it is reduced effectively to 0.06 for both $u_{sup} = 0.075$ m s^{-1} and 0.75 m s^{-1}, which is 10 times lower than that of the low supply air speed. Generally, dilution is an increasing function with supply air speed, and tends to constant with certain supply air speed for fixed emission of pollutant source.

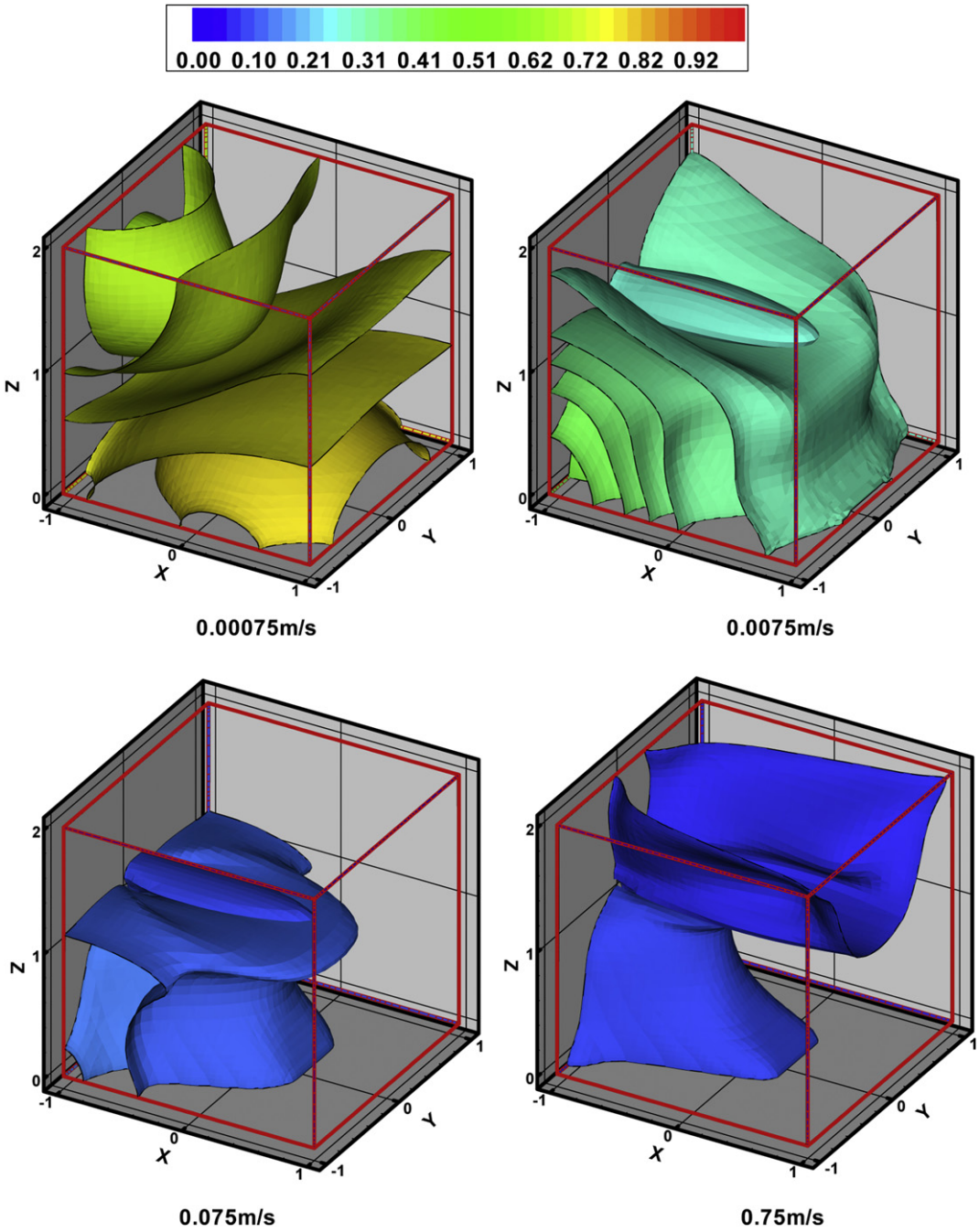

Fig. 6 – Predicted concentration contours of carbon dioxide with various supply air speed for fresh air ratio $r = 0.5$ and filtered removal efficiency $r_e = 0$.

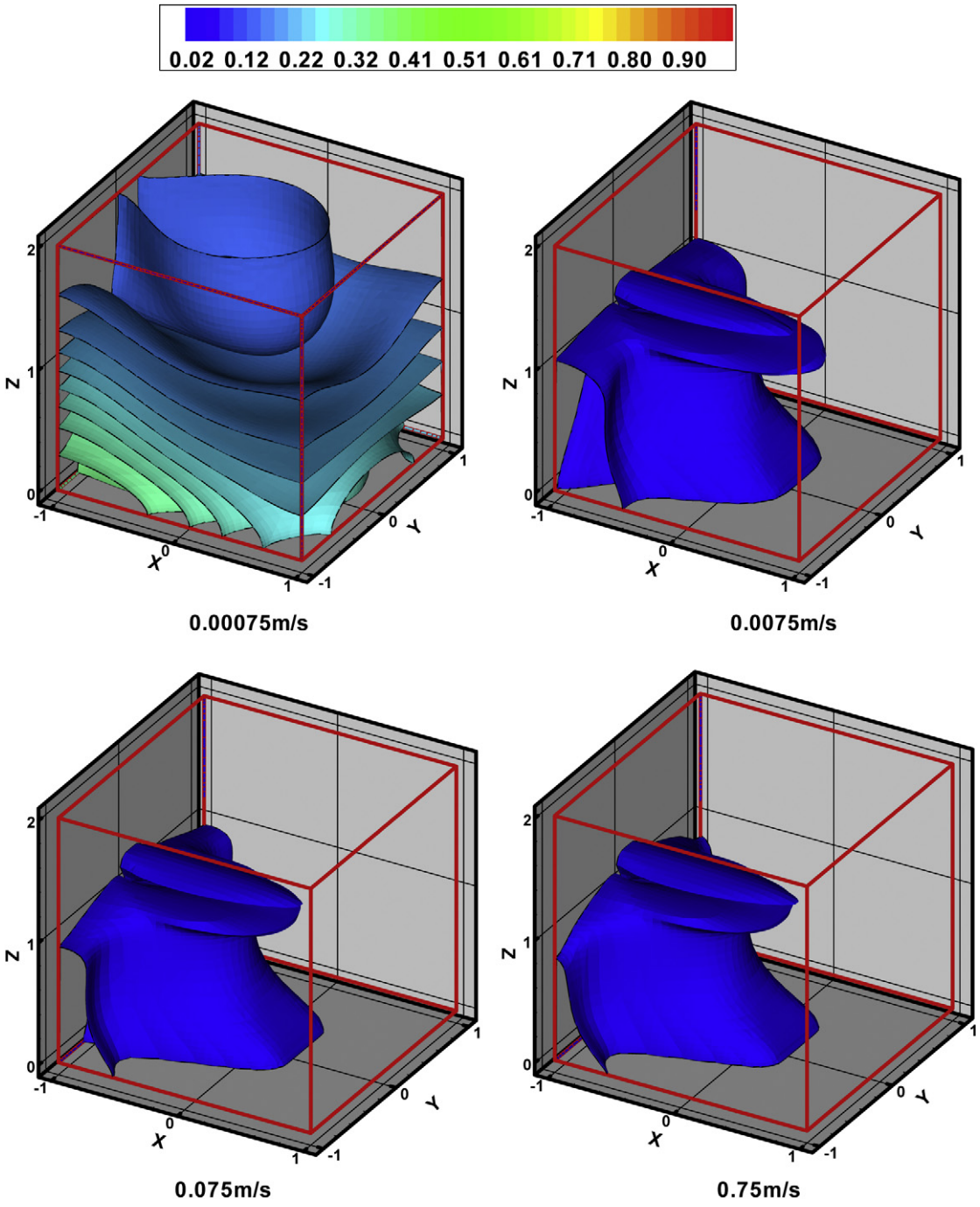

Fig. 7 – Predicted concentration contours of formaldehyde with various supply air speed for fresh air ratio $r = 0.5$ and filtered removal efficiency $r_e = 0.8$.

Fig. 7 illustrates typical cross-section contours of formaldehyde with various supply air speed for fresh air ratio $r = 0.5$ and filtered removal efficiency $r_e = 0.8$. These spatial contours reveal that with filtered removal efficiency being 80%, the inlet coming wind always brings the low concentration level even $u_{sup} = 7.5 \times 10^{-4}$ m s^{-1}. The formaldehyde concentration distributions are similar each other for supply air speed greater than 0.0075 m s^{-1}. Besides, this result is reasonable also because the emission factor of formaldehyde is 1 order of magnitude greater than that of carbon dioxide.

The effect of supply air speed on the average pollutant level is indicated in Fig. 8, which directly shows the variation of the indoor pollutant level. Firstly, increasing supply air speed results in increasing air flow rate thus effectively reducing the indoor pollutant concentration. However, formaldehyde and carbon dioxide levels would asymptotically tend to constants respectively if the supply air speed is higher than 0.0075 m s^{-1} and 0.75 m s^{-1} with and without filtration effects. This is due to the fact that the pollutant distribution maintains invariant even when supply air speed exceeds 0.75 m s^{-1}, which is

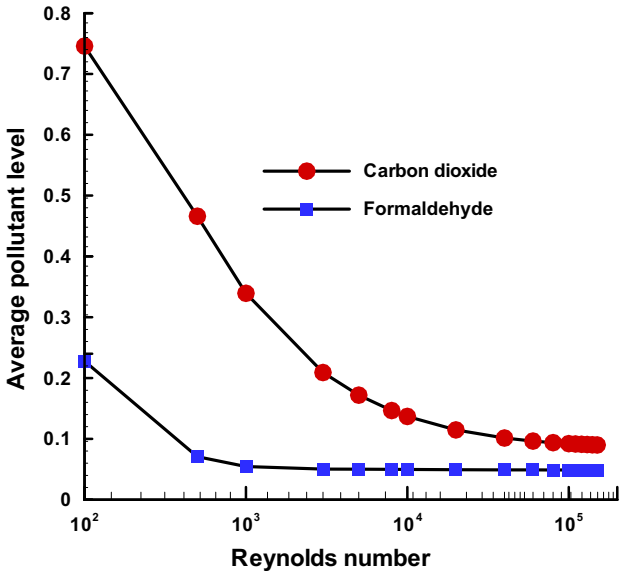

Fig. 8 – Variation of volume-average pollutant level with supply air speed as parameter for fresh air ratio $r = 0.5$ and filtered removal efficiency $r_e = 0.8$.

irrespective of carbon dioxide or formaldehyde. Actually, as the supply air speed increases further exceeding 0.75 m s^{-1}, the indoor flow structure changes little, which results in the invariant average pollutant level in the building.

3.2. *Effect of fresh air ratio*

The supply air speed and recirculation filter removal fraction keep constants of 0.75 m s^{-1} and 0.8, respectively. The range of the required fresh air ratio is from 0 to 1, i.e., the supply airflow ranges from the whole recirculation to total fresh air.

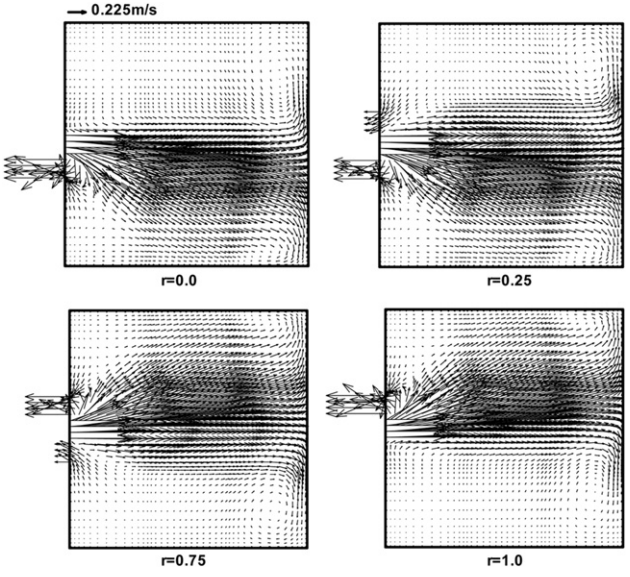

Fig. 9 – Predicted horizontal flow vectors at the center of the supplying air port ($Z = 1.125$) with various fresh air ratio r, whereas supply air speed 0.75 m s^{-1} and filtered removal efficiency $r_e = 0.8$ are maintained.

Fig. 9 displays the predicted horizontal vectors at the center of the supply port ($Z = 1.125$) with various fresh air ratio r. For $r = 0$, the recirculation port results in the strong indraft being confined within some narrow zone. The nearby area, however, is not entrained significantly. With increasing fresh air ratio, the increasing velocity of the exhaust port results in the enlargement of the confined zone. For fresh air ratio values approaching to 0.5, shown in the Fig. 5(b), the fluid flow accelerates. Moreover, the path followed by the pathlines from the inlet to the outlet and recirculation port changes as the speed of the inlet airflow increases. In general, the tendency is to close the pathlines to the walls. Note how the flow traps the contaminant in the front region of the enclosure. Inside the jet region, the pollutant concentration is always lower than 10% of the maximum found in the enclosure. This is due to the fact that the incoming clean air bypasses the rest of the enclosure and proceeds directly toward the outlet. As the fresh air ratio increases, a weak counterclockwise cell develops in the front left corner, while the incoming jet stretches (becomes straighter and thinner) near the back of the enclosure.

The numbers listed on the pollutant contours in Figs. 10 and 11 represent the values of the dimensionless concentration C. High C values represent high concentrations corresponding to the contaminated fluid, while C values close to 0 represent flow regions that have been effectively cleaned by the through-flow. Worth noting is that the region that is the last to be cleaned of contaminant fluid coincides with the central zone of the slow recirculation illustrated by the pathline patterns in the steady state. Figs. 10 and 11 illustrate that the changes occur in the CO_2 and formaldehyde concentration fields respectively when the fresh air ratio increases from 0 to 1. It can be found that the role of the fresh air is to dilute the indoor pollutants. Observing from Fig. 10, for fresh air ratio $r = 0.0$, the concentration of carbon dioxide is unity in the whole room. With no fresh air and filtration, all the incoming flow is of high concentration and re-circulates within the room, and the accumulation occurs markedly. With increasing the fresh air ratio, $r = 0.25$, the incoming flow concentration is clearly decreased to about 0.25 at the supply location. But it is reduced effectively to 0.06 as the fresh air ratio increases to 0.5 shown in Fig. 6. The situations for higher fresh air ratio just make the same sense. This is more clearly if the contaminant is filtered with $r_e = 0.8$. Observing from Fig. 11, even without the fresh air, the indoor pollutant (formaldehyde) concentration is acceptable. This means that the fresh air and filtration are both the effective ways to improve the indoor air environment.

The variation of average pollutant level with fresh air ratio r as parameter for supply air speed keeping 0.75 m s^{-1} is presented in Fig. 12 with or without filtration. An initial, almost linear variation of the average pollutant level prevails when the contaminant is carried away by the jet, and the removal efficiency represented as the reciprocal of average pollutant level increases abruptly. Without filtration, the concentration of carbon dioxide is markedly dropped. Thereafter, a small decrease of carbon dioxide concentration is observed. The carbon dioxide concentration is consistently

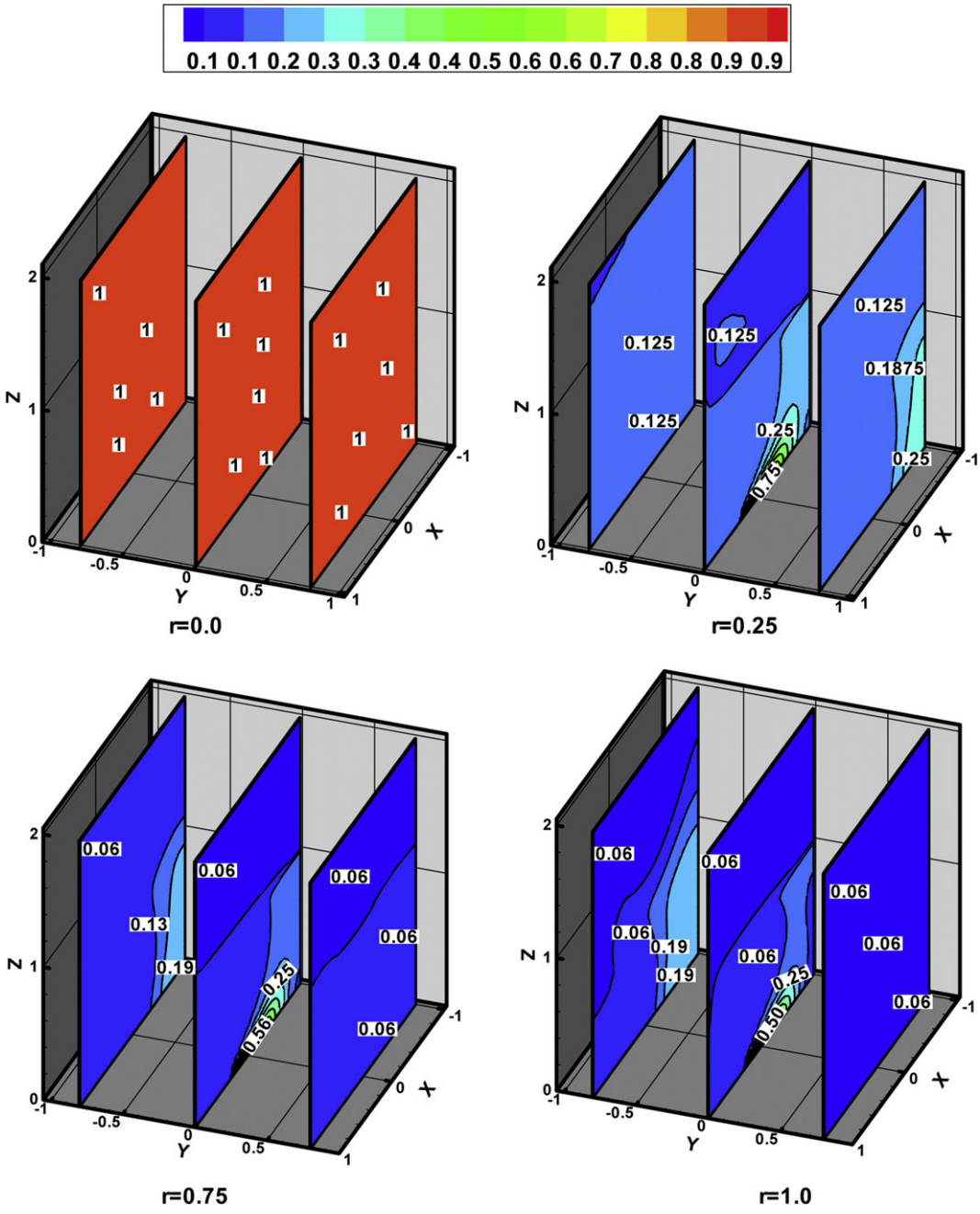

Fig. 10 – Predicted concentration slices of carbon dioxide with various fresh air ratio *r* as the supply air speed maintains at 0.75 m s^{-1} and non-filtration is assumed.

decreasing in order of increasing fresh air ratio, but the decreasing rate becomes less. While, the concentration of formaldehyde under filtration condition (r_e = 0.8) is first slightly decreasing until fresh air ratio is 0.5, which is the minimal pollutant level, and then increasing. The highest average formaldehyde level is about 0.09, much lower than that of carbon dioxide without filtration. The optimum value for fresh air ratio is about 0.5, which coincides with the conclusion made by Elkilani and Bouhamra (2001).

The average pollutant level with or without filtration differs less for high fresh air ratio, and approaches the same level with fresh air ratio r = 1.0. It is due to the fact that the indoor contaminant level cannot be zero even under total fresh air operation (r = 1.0), which may attribute to the continuous release of the contaminant. The numerical result for r = 1.0 also agrees well with the overall constituent conservation analysis presented in Eq. (A8) (See the Appendix).

3.3. *Effect of filtered removal efficiency*

The fresh air ratio and supply air speed are maintained at 0.5 and 0.75 m s^{-1} respectively. The range of required filtered removal efficiency is from 0.0 to 1.0. The objective is to

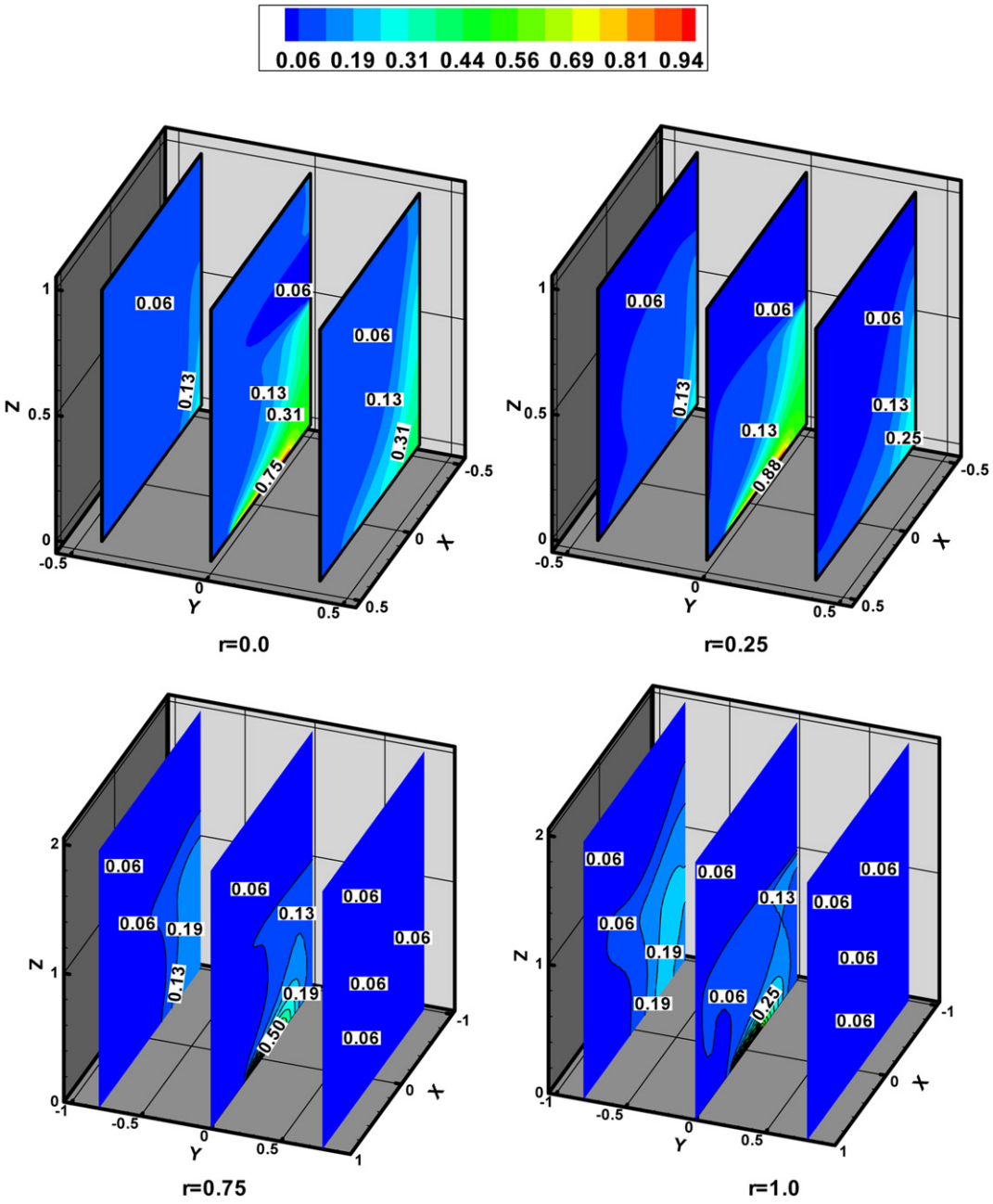

Fig. 11 – Predicted concentration slices of formaldehyde with various fresh air ratio *r* as the supply air speed maintains at 0.75 m s^{-1} and filter removal efficiency *re* maintains at 0.8.

investigate the impact of the filtered removal efficiency on the pollutant intensity and on the emission rates of the selected pollutant. For carbon dioxide cannot be filtered, this section focuses on formaldehyde.

The concentration of formaldehyde is presented in Fig. 13 for four different filtered removal efficiencies. An area of higher concentration in recycling region is due to the interaction of the primary and secondary flow cells. The simulation results show that formaldehyde emitted from the floor tends to follow the course of the airflow field moving circularly. It can be seen that the minimum is at the inlet and quickly increases along the length. We can see a higher and uniform concentration distribution after $X = 0$. Observing from Fig. 13, the formaldehyde concentration is a step increasing function for filtered removal efficiency r_e as parameter. The lower the filtered removal efficiency, the more the pollutant will be accumulated within the building. The double peak structures are observed in Y-direction concentration profiles. The both two peaks are corresponding to return and exhausting ports. We can see that the accumulation occurs not only on the floor, but also on the recirculating and exhausting sides. The Z-direction concentration profiles indicate the sharply decreasing just above the floor, and then slowly decreasing along the height.

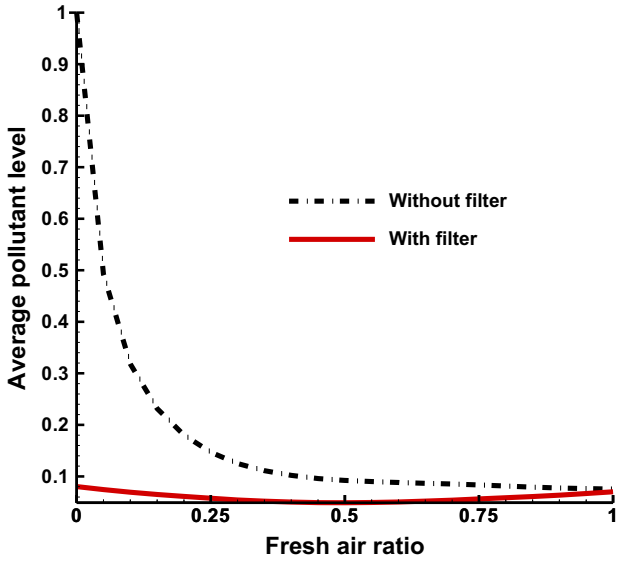

Fig. 12 – Variation of volume-average pollutant level with fresh air ratio r as parameter as the supply air speed is maintained at 0.75 m s^{-1} and the filtered removal efficiency is maintained at $r_e = 0.8$.

Fig. 14 presents the volumetric average formaldehyde level and emission rate as a function of filtered removal efficiency. With an increase in the filtered removal efficiency, the average concentration decreases. This means that the higher filtered removal efficiency, the less pollutant can penetrate into the building. The emission rate of formaldehyde is also affected by the filtered removal efficiency. Reversing from the volumetric average concentration, the emission rate is an increasing function with the filtered removal efficiency.

3.4. *Effect of thermal buoyancy*

The Archimedes number, ranging from 0 to 0.8, is considered here. Correspondingly, the maximal temperature difference between the heat source and the supply air is 6.3 K. The supply air speed, fresh air ratio r, and filtered removal efficiency r_e are maintained at 0.75 m s^{-1}, 0.5 and 0.8 respectively. Thus, the buoyant strength analysis would be conducted to illustrate the relations between the air quality and the airflow pattern under the situation of mixed ventilation.

To examine the effect of thermal plume to contaminant transportation, Fig. 15 presents the dimensionless iso-

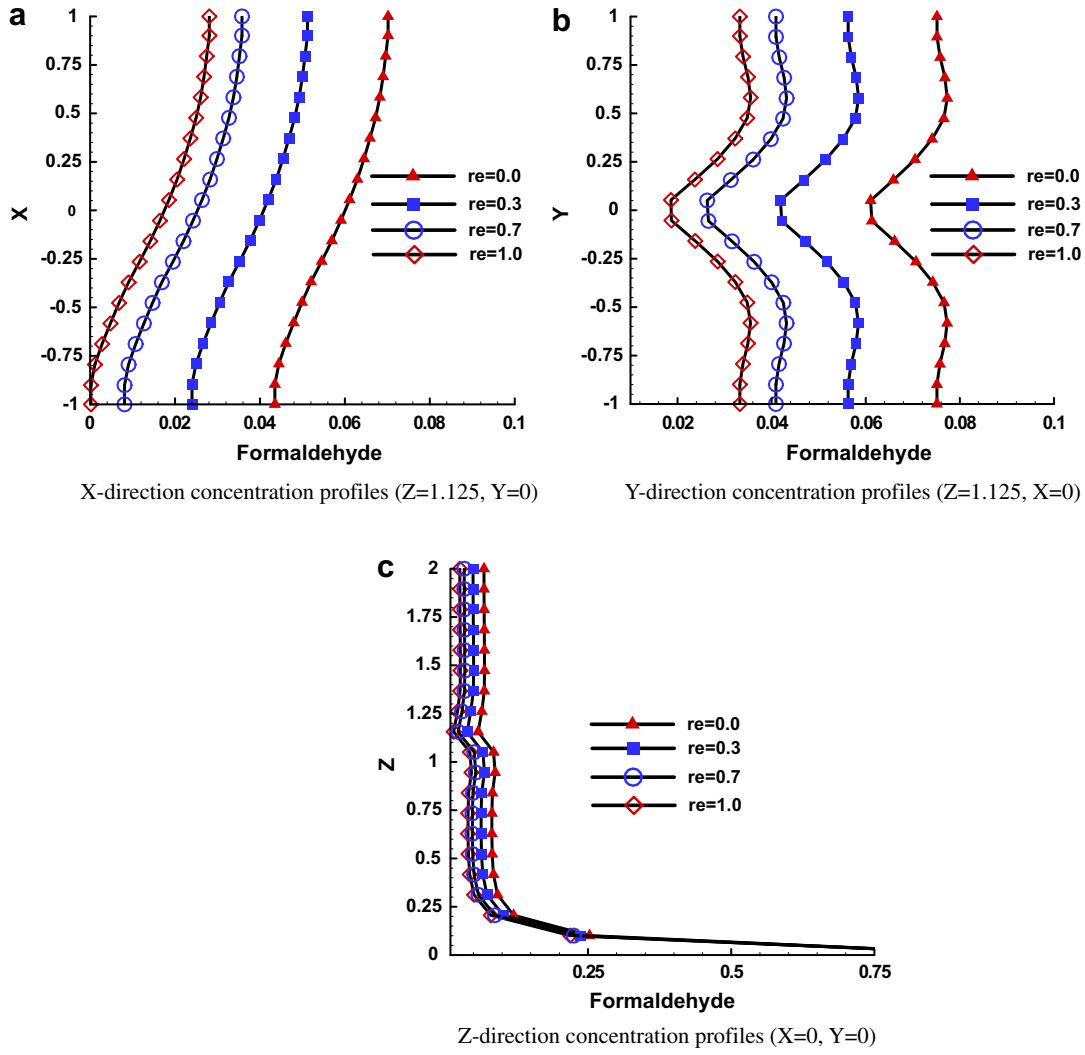

X-direction concentration profiles (Z=1.125, Y=0)

Y-direction concentration profiles (Z=1.125, X=0)

Z-direction concentration profiles (X=0, Y=0)

Fig. 13 – Evolution of center concentration profiles of formaldehyde for various filtered removal efficiency, including X-direction (a), Y-direction (b) and Z-direction (c) concentration profiles.

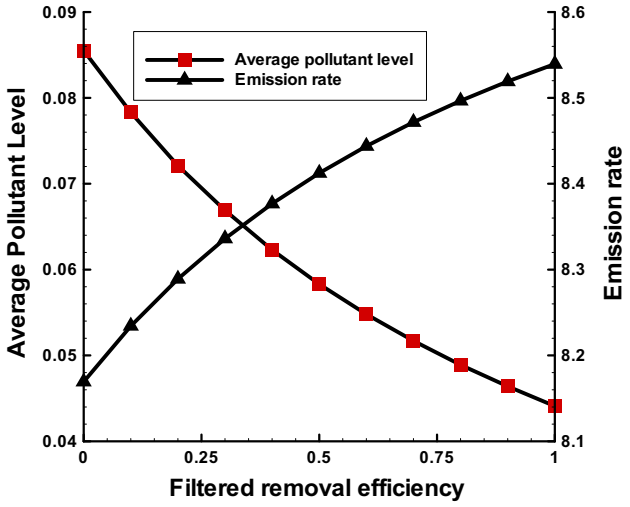

Fig. 14 – The volume-average pollutant level and emission rate of formaldehyde as functions of filtered removal efficiencies as Re = 10^5 (u_{sup} = 0.75 m s^{-1}) and fresh air ratio r = 0.5 are maintained.

concentration contours of CO_2. When the thermal buoyancy is not imposed (Ar = 0.0), a circulation is formed with a large eddy covering the lower half room and the reverse flow caused by the pressure difference occupies the upper portion for the room centerline (Y = 0.0). This flow structure is completely identical to that presented in Fig. 5(a) with supply air speed of 0.75 m s^{-1}, since the indoor-generated heat is passively transported by the forced air flow, and thermal plume does not influence the airflow pattern.

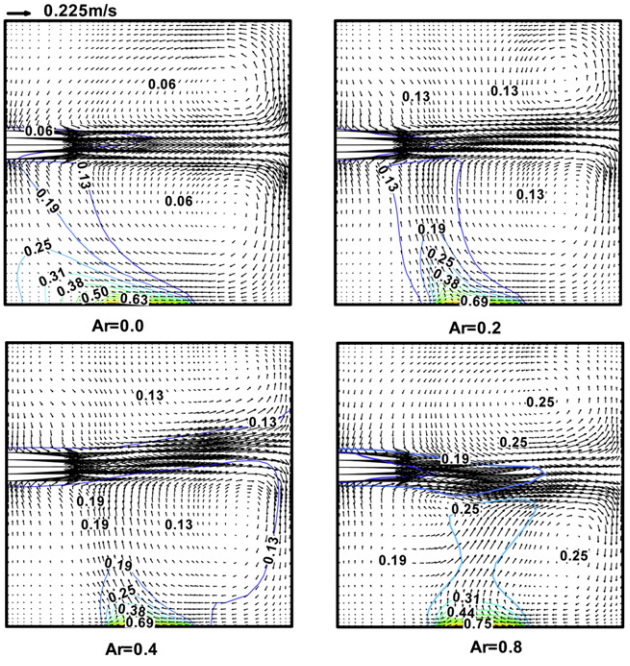

Fig. 15 – Iso-concentration contours of CO_2 and flow velocity vector plot at Y = 0.0 (the room centerline) varying with Gr/Re^2 (Ar), whereas the supply air speed, fresh air ratio r, and filtered removal efficiency r_e are maintained at 0.75 m s^{-1}, 0.5 and 0.8 respectively.

As the thermal buoyancy initiates (Ar > 0), the flow field would be dynamically affected by the thermal plume. However, when Ar is low, such as 0.2 (the corresponding temperature difference is 1.73 K), the thermal plume becomes just in front of the heat source as illustrated in Fig. 15. Part of the contaminant source exhausts pollutant directly with the thermal plume before being induced with cooling supply air jet and transported through the whole room. Although the dominant air circulation in the room is not changed considerably due to the weak thermal buoyancy, the contaminant release is enhanced and consequently the indoor air environment becomes worse.

In typical commercial buildings where mechanical ventilation systems are used, the airflow pattern is dominated by the supply diffuser jet and the thermal plumes. As Ar is no more than 0.3, the supply jet still has a sufficient momentum to reach the opposite wall. As heat source strength increases further, the effect of the thermal plume on the fluid flow is clearly strengthened as presented in Fig. 15 with Ar = 0.4. The supply jet detaches sooner and rises up to the ceiling. This change causes a large part of the room to be exposed to air environment with contaminant concentration being higher than the preceding situations. When the temperature difference increases to 6.93 K (Ar = 0.8), multiple circulating cells appear in the room area far away from the diffuser, where the pollutant accumulates and the effect of ventilation becomes poor. The supply jet detaches much sooner and drop to the occupied zone causing drafts and different airflow patterns. The thermal enhanced diffusion also occurs for formaldehyde dispersion, but it is weaker than CO_2 for filtration effect.

4. Conclusions

Increasing outdoor airflow rate reduces indoor pollutant level. However, increasing outdoor airflow rate increases the cooling load of the building. A numerical model of indoor air quality is developed based on atmospheric convection diffusion equations and RSM turbulent model to predict the pollutant concentrations within a building equipped with a novel window-type air conditioner. The effects of air supplying, recirculation, filtration, and thermal buoyancy are also included.

Sensitivity analysis shows that increasing air velocity reduces the indoor pollutant levels effectively. However, the volumetric contaminant concentration is almost constant when supply air speed exceeds 0.75 m s^{-1}.

The concentration of pollutants with different molecular diffusivity asymptotically approaches to the same value as the fresh air ratio tends to be unity. However, it is a relatively small value as the fresh air ratio equals unity, and the numerical result agrees well with the overall conservation analysis of pollutant constituents.

The indoor formaldehyde level is a decreasing function with filtered removal efficiency, whereas the emission rate is an increasing function with the filtered removal efficiency. Increasing the fresh air ratio and filtration efficiency would significantly improve the indoor air environment simultaneously.

The thermal buoyancy has a strong effect on the spatial distribution of the contaminants. Thermal plume not only affects the air flow pattern, but also enhances the pollutant dispersions. Consequently, it tends to increase indoor pollutant concentration.

Acknowledgments

This work was partially supported by Natural Science Foundation of China (NO. 50578059), Key Talent Plan of Hunan University of Technology (2010–2015), Key Project of Science and Technology in Hunan Province – Key Technologies and Integrations of Air Purification in Industrial Halls (NO. 2010FJ1012-1), Twelve-Five National Supportive Plan from China Ministry of Science and Technology – integration and demonstration of key building energy conservations in hot summer and cold winter regions in China (NO. 2011BAJ03B07), and Alexander von Humboldt Foundation with host - Prof. Ernst Rank's research group in TUM, Germany (2011–2013).

Appendix A

Residential room floor source is assumed to release carbon dioxide and formaldehyde uniformly with time and with an assumption of mixing with fully developed return air. The outdoor fresh air does not contain carbon dioxide and formaldehyde. Plus, the indoor initial concentration of the both pollutants $C_0 = 0$. In fact, the difference between the recirculation air and mixing air maintains constant. The realistic air conditioning operation with recirculation air and injected fresh air could be indicated as follows,

(1) For the first recirculation

$$C_1 = \delta C \tag{A1}$$

$$C_{\text{mix }1} = \frac{C_1(1-r)(1-r_e)Q_{\text{sup}} + C_o r Q_{\text{sup}}}{Q_{\text{sup}}}, \quad \text{but if } C_0 = 0 \tag{A2}$$

$$\text{Thus, } C_{\text{mix }1} = C_1(1-r)(1-r_e) \tag{A3}$$

(2) For the second recirculation

$$C_2 = C_{\text{mix }1} + \delta C = C_1(1-r)(1-r_e) + C_1 = C_1\sum_{k=0}^{1}[(1-r)(1-r_e)]^k \tag{A4}$$

$$C_{\text{mix }2} = C_2(1-r)r_e + \delta C = [C_1(1-r)r_e + C_1](1-r)r_e + C_1 = C_1\sum_{k=0}^{2}[(1-r)r_e]^k \tag{A5}$$

(3) For nth recirculation

$$C_n = C_{\min(n-1)} + \delta C = C_1\sum_{i=0}^{n-1}[(1-r)(1-r_e)]^i = C_1\frac{[(1-r)(1-r_e)]^{n-1}-1}{(1-r)(1-r_e)-1} \tag{A6}$$

$$C_{\text{mix}(n)} = C_n(1-r)(1-r_e) + \delta C = C_1\sum_{i=0}^{n}[(1-r)(1-r_e)]^i \tag{A7}$$

If n asymptotically tends to the infinite, the indoor and mixed concentration of pollutant are exactly the same and should be given by

$$\lim_{n\to\infty} C_n = \lim_{n\to\infty} C_{\text{mix}(n)} = \frac{C_1}{1-(1-r)(1-r_e)} \tag{A8}$$

Here C_1 represents the concentration of recirculating port for the first recirculation. With aforementioned temporal constant releasing assumptions, even if C_1 is the first recirculation and small value, it will not be zero anyway.

Additionally, Eq. (A8) demonstrates that the steady concentration of indoor pollutant is inversely proportional to the fresh air ratio r as filtered removal efficiency r_e is set zero. It is worth noting that no matter what the values of r and r_e, even if both of the fresh air ratio and filter removal efficiency are set unity, the pollutant concentration within the room would be C_1, whereas not zero.

REFERENCES

Abadie, M., Limam, K., Allard, F., 2001. Indoor particle pollution: effect of wall textures on particle deposition. Build. Environ. 36, 821–827.

Abadie, M., Limam, K., Bouilly, J., Genin, D., 2004. Particle pollution in the French high-speed train (TGV) smoker cars: measurement and prediction of passengers' exposure. Atmos. Environ. 38, 2017–2027.

Aglan, H.A., 2003. Prediction model for CO_2 generation and decay in building envelopes. J. Appl. Phys. 93, 1287–1290.

Béghein, C., Haghighat, F., Allard, F., 1992. Numerical study of double-diffusive natural convection in a square cavity. Int. J. Heat Mass Transf. 35, 833–846.

Béghein, C., Jiang, Y., Chen, Q.Y., 2005. Using large eddy simulation to study particle motions in a room. Indoor Air 15, 281–290.

Bolashikov, Z.D., Melikov, A.K., 2009. Methods for air cleaning and protection of building occupants from airborne pathogens. Build. Environ. 44, 1378–1385.

Bouhamra, W.S., Elkilani, A.S., 1999. Development of a new model for the estimation of indoor volatile organic compounds concentration based on experimental sorption parameters. Environ. Sci. Technol. J. 33, 2100–2105.

Bouhamra, W.S., Elkilani, A.S., Raheem, M.Y., 1998. Predicted and measured air exchange rates. ASHRAE J. 40, 42–45.

Buhamra, S.S., Bouhamra, W.S., Elkilani, A.S., 1998. Assessment of air quality in ninety-nine residences of Kuwait. Environ. Technol. 19, 357–368.

Elkilani, A., Bouhamra, W.S., 2001. Estimation of optimum requirements for indoor air quality and energy consumption in some residences in Kuwait. Environ. Int. 27, 443–447.

Fehrm, M., Reiners, W., Ungemach, M., 2002. Exhaust air heat recovery in buildings. Int. J. Refrigeration 25, 439–449.

Gao, N.P., Niu, J.L., 2007. Modeling particle dispersion and deposition in indoor environments. Atmos. Environ. 41, 3862–3876.

Haghighat, F., Lee, C.S., Pant, B., Bolourani, G., et al., 2008. Evaluation of various activated carbons for air cleaning – towards design of immune and sustainable buildings. Atmos. Environ. 35, 8176–8184.

Hays, S.M., Gobbel, R.V., Ganick, N.R., 1995. Indoor Air Quality: Solution and Strategies. Mc Graw-Hill, Washington D.C.

Huppert, H.E., Sparks, R.S.J., 2006. Extreme natural hazards: population growth, globalization and environmental change. Philos. Trans. R. Soc. A 364, 1875–1888.

Koseff, J.R., Street, R.L., 1984. The lid-driven cavity flow: a synthesis of qualitative and quantitative observations. ASME J. Fluid Eng. 106, 390–398.

Lai, A.C.K., Chen, F., 2006. Modeling particle deposition and distribution in a chamber with a two-equation Reynolds-averaged Navier–Stokes model. J. Aerosol Sci. 37, 1770–1780.

Li, F., Niu, J.L., 2007. Control of volatile organic compounds indoors – Development of an integrated mass-transfer-based model and its application. Atmos. Environ. 41, 2344–2354.

Liang, C.H., Zhang, L.Z., Pei, L.X., 2010. Independent air dehumidification with membrane-based total heat recovery: modeling and experimental validation. Int. J. Refrigeration 33, 398–408.

Liu, D., Tang, G.F., Zhao, F.Y., 2006. Modeling and experimental investigation of looped separate heat pipe as waste heat recovery facility. Appl. Therm. Eng. 26, 2433–2441.

Liu, D., Zhao, F.Y., Tang, G.F., 2007. Frosting of heat pump with heat recovery facility. Renew. Energy 32, 1228–1242.

Liu, D., Zhao, F.Y., Tang, G.F., 2008a. Modeling and performance investigation of a closed-type thermoelectric clothes dryer. Dry. Technol. 26, 1208–1216.

Liu, D., Zhao, F.Y., Tang, G.F., 2008b. Conjugate heat transfer in an enclosure with centered conducting body imposed sinusoidal temperature profiles on one side. Numer. Heat Transf. Part A 53, 204–223.

Liu, D., Zhao, F.Y., Tang, G.F., 2008c. Numerical analysis of two contaminants removal from a three-dimensional cavity. Int. J. Heat Mass Transf. 51, 378–382.

Liu, D., Zhao, F.Y., Tang, G.F., 2008d. Thermosolutal convection in a saturated porous enclosure with concentrated energy and solute sources. Energ. Convers. Manag. 49, 16–31.

Liu, D., Zhao, F.Y., Tang, G.F., 2010a. Active low-grade energy recovery potential for building energy conservation. Renew. Sustain. Energy Rev. 14, 2736–2747.

Liu, D., Zhao, F.Y., Tang, G.F., 2010b. Non-unique convection in a three-dimensional slot-vented cavity with opposed jets. Int. J. Heat Mass Transf. 53, 1044–1056.

Longest, P.W., Vinchurkar, S., Martonen, T., 2006. Transport and deposition of respiratory aerosols in models of childhood asthma. J. Aerosol Sci. 37, 1234–1257.

Moureh, J., Flick, D., 2004. Airflow pattern and temperature distribution in a typical refrigerated truck configuration loaded with pallets. Int. J. Refrigeration 27, 464–474.

Moureh, J., Flick, D., 2005. Airflow characteristics within a slot-ventilated enclosure. Int. J. Heat Fluid Flow 26, 12–24.

Moureh, J., Tapsoba, J., Derens, E., Flick, D., 2009. Air velocity characteristics within vented pallets loaded in a refrigerated vehicle with and without air ducts. Int. J. Refrigeration 32, 220–234.

Nguyen, A., Kim, Y., Shin, Y., 2005. Experimental study of sensible heat recovery of heat pump during heating and ventilation. Int. J. Refrigeration 28, 242–252.

Patankar, S.V., 1980. Numerical Heat Transfer and Fluid Flow. Hemisphere Publishing Co., Washington.

Smale, N.J., Moureh, J., Cortella, G., 2006. A review of numerical models of airflow in refrigerated food applications. Int. J. Refrigeration 29, 911–930.

Versteeg, H.K., Malalasekera, W., 1996. An Introduction to Computational Fluid Dynamics. Longman Group Ltd., London.

Wargocki, P., Fanger, P.O., Krupicz, P., Szczecinski, A., 2004. Sensory pollution loads in six office buildings and a department store. Energ. Buildings 36, 995–1001.

Yang, X., Chen, Q., 2001. A mass transfer model for simulating VOC sorption on building materials. Atmos. Environ. 35, 257–269.

Yu, B.F., Hu, Z.B., Liu, M., et al., 2009. Review of research on air-conditioning systems and indoor air quality control for human health. Int. J. Refrigeration 32, 3–20.

Zhang, Z., Chen, Q., 2006. Experimental measurements and numerical simulations of particle transport and distribution in ventilated rooms. Atmos. Environ. 40, 3396–3408.

Zhao, F.Y., Liu, D., Tang, G.F., 2007. Application issues of the streamline, heatline and massline for conjugate heat and mass transfer. Int. J. Heat Mass Transf. 50, 320–334.

Zhao, F.Y., Liu, D., Tang, G.F., 2008. Natural convection in an enclosure with localized heating and salting from below. Int. J. Heat Mass Transf. 51, 2889–2904.

Zhao, F.Y., Liu, D., Tang, G.F., 2010. Determining boundary heat flux profiles in an enclosure containing solid conducting block. Int. J. Heat Mass Transf. 53, 1269–1282.

Zhao, F.Y., Liu, D., Tang, L., Ding, Y.L., Tang, G.F., 2009. Direct and inverse mixed convections in an enclosure with ventilation ports. Int. J. Heat Mass Transf. 52, 4400–4412.

Zhao, F.Y., Liu, D., Wang, H.Q., Kou, G.X., Tang, G.F., 2011. Free heat and mass transfer in a porous enclosure with side vents. Dry. Technol. 29, 91–104.